AGU PUBLICATIONS

JGR

Journal of Geophysical Research: Space Physics

RESEARCH ARTICLE

10.1002/2014JA020364

Key Points:
- The frequency gas of banded chorus is explained by linear dispersion theory
- Banded chorus is excited by two distinct anisotropic electron components
- Theory, simulations, and observations agree

Correspondence to:
X. Fu,
xrfu@lanl.gov

Citation:
Fu, X., et al. (2014), Whistler anisotropy instabilities as the source of banded chorus: Van Allen Probes observations and particle-in-cell simulations, *J. Geophys. Res. Space Physics*, *119*, 8288–8298, doi:10.1002/2014JA020364.

Received 8 JUL 2014
Accepted 23 SEP 2014
Accepted article online 27 SEP 2014
Published online 22 OCT 2014

Whistler anisotropy instabilities as the source of banded chorus: Van Allen Probes observations and particle-in-cell simulations

Xiangrong Fu[1], Misa M. Cowee[1], Reinhard H. Friedel[1], Herbert O. Funsten[1], S. Peter Gary[2], George B. Hospodarsky[3], Craig Kletzing[3], William Kurth[3], Brian A. Larsen[1], Kaijun Liu[4], Elizabeth A. MacDonald[5], Kyungguk Min[4], Geoffrey D. Reeves[1], Ruth M. Skoug[1], and Dan Winske[1]

[1]Los Alamos National Laboratory, Los Alamos, New Mexico, USA, [2]Space Science Institute, Boulder, Colorado, USA, [3]Department of Physics and Astronomy, University of Iowa, Iowa City, Iowa, USA, [4]Department of Physics, Auburn University, Auburn, Alabama, USA, [5]NASA/Goddard Space Flight Center, Greenbelt, Maryland, USA

Abstract Magnetospheric banded chorus is enhanced whistler waves with frequencies $\omega_r < \Omega_e$, where Ω_e is the electron cyclotron frequency, and a characteristic spectral gap at $\omega_r \simeq \Omega_e/2$. This paper uses spacecraft observations and two-dimensional particle-in-cell simulations in a magnetized, homogeneous, collisionless plasma to test the hypothesis that banded chorus is due to local linear growth of two branches of the whistler anisotropy instability excited by two distinct, anisotropic electron components of significantly different temperatures. The electron densities and temperatures are derived from Helium, Oxygen, Proton, and Electron instrument measurements on the Van Allen Probes A satellite during a banded chorus event on 1 November 2012. The observations are consistent with a three-component electron model consisting of a cold (a few tens of eV) population, a warm (a few hundred eV) anisotropic population, and a hot (a few keV) anisotropic population. The simulations use plasma and field parameters as measured from the satellite during this event except for two numbers: the anisotropies of the warm and the hot electron components are enhanced over the measured values in order to obtain relatively rapid instability growth. The simulations show that the warm component drives the quasi-electrostatic upper band chorus and that the hot component drives the electromagnetic lower band chorus; the gap at $\sim\Omega_e/2$ is a natural consequence of the growth of two whistler modes with different properties.

1. Introduction

The recently launched Van Allen Probes mission to Earth's magnetosphere is dramatically demonstrating the importance of wave-particle processes in the radiation belts [*Reeves et al.*, 2013]. The Electric and Magnetic Field Instrument Suite and Integrated Science (EMFISIS) Waves instruments [*Kletzing et al.*, 2013] aboard the twin satellites of this mission are providing significant new information about large-amplitude magnetospheric chorus, a phenomenon which has been observed by many spacecraft (see the review by *Thorne* [2010]), but which only recently has been convincingly demonstrated to make important contributions to magnetospheric electron acceleration [*Thorne et al.*, 2013].

Enhanced amplitude chorus often arises in two distinct frequency bands (therefore called "banded chorus"), the lower band $0.1 < \omega_r/\Omega_e < 0.5$ and the upper band $0.5 < \omega_r/\Omega_e < 0.8$ [*Meredith et al.*, 2001, 2012; *Santolík et al.*, 2003, 2014], where Ω_e represents the electron cyclotron frequency. This gap between the two bands does not correspond to any characteristic frequency described by cold plasma theory and has not yet been given a fully satisfactory explanation [e.g., *Sazhin and Hayakawa*, 1992; *Liu et al.*, 2011, and references therein]. Some competing theories have been proposed to explain the banded chorus properties. *Omura et al.* [2009] developed a nonlinear wave growth theory for magnetospheric chorus, taking into account the spatial inhomogeneity of the background magnetic field, and used their theory to explain the gap at $\sim 0.5\Omega_e$ as a result of the nonlinear damping of a slightly oblique whistler wave packet propagating away from the magnetic equator along the inhomogeneous magnetic field. This theory has recently been applied to explain some chorus observations [e.g., *Kurita et al.*, 2012; *Habagishi et al.*, 2014]. Other studies on banded chorus explored effects such as nonlinear wave-wave coupling [*Schriver et al.*, 2010] and cold plasma density variation [*Bell et al.*, 2009].

Recently, *Li et al.* [2010] found that electron velocity distributions observed from Time History of Events and Macroscale Interactions during Substorms satellites during periods of banded chorus may have temperature anisotropies $T_\perp/T_\parallel > 1$ (where $\perp$ and $\parallel$ denote directions perpendicular and parallel, respectively, to the background magnetic field) both above ~10 keV and below ~2 keV but that electrons with intermediate energies are more nearly isotropic. Similar features of electron phase space density were also observed by Combined Release and Radiation Effects Satellite [*Thorne et al.*, 2010]. *Santolík et al.* [2010] used kinetic linear dispersion theory to study a banded chorus case observed by the Cluster spacecraft and showed that highly anisotropic ($T_\perp/T_\parallel > 10$) injected electrons at energies of a few hundred eV to a few keV could drive the upper band chorus; but their model of trapped electrons at energies above 10 keV gave insufficient growth of the lower band. A related particle-in-cell (PIC) simulation by *Schriver et al.* [2010] also based on Cluster electron observations showed that 300 eV anisotropic electrons indeed drove upper band whistlers unstable but that the lower band is generated by nonlinear wave-wave coupling. *Liu et al.* [2011] carried out further PIC simulations based upon typical magnetospheric parameters showing that warm (below 1 keV) and hot (above 10 keV) electron components with sufficiently large temperature anisotropies could drive both lower band and upper band whistler instabilities relatively independent of each other.

Previous studies of chorus excitation had to rely on assumed plasma conditions because accurate measurements of the plasma environment were not available. The Van Allen Probes mission was designed, in part, to make the measurements required to quantitatively test theories of wave generation. The Helium, Oxygen, Proton, and Electron (HOPE) mass spectrometer of the Van Allen Probes mission measures the ion and electron fluxes at each of the two spacecraft within the terrestrial radiation belts over the energy range from 10 eV to 50 keV [*Funsten et al.*, 2013; *Spence et al.*, 2013]. This energy range encompasses the electrons which are the likely drivers of large-amplitude magnetospheric chorus, which has its source in the whistler anisotropy instability [e.g., *MacDonald et al.*, 2008, and references therein] driven by the electron $T_\perp/T_\parallel > 1$. Now for the first time, with simultaneous measurements of the chorus wave environment by EMFISIS and detailed electron velocity distributions from a few eV to MeV by HOPE, we can perform simulations with inputs based on the actual, observed conditions.

HOPE instrument measurements from Van Allen Probes spacecraft A during a banded chorus event associated with a geomagnetic storm on 1 November 2012 (as well as several other such events not described here) indicate $T_\perp > T_\parallel$ anisotropies at a few hundred eV and a few keV energies. We assume that we may fit the electron distribution with bi-Maxwellians to provide the input conditions for our linear dispersion solver and PIC simulations. Our fits yield a cold (few tens of eV) population, a warm (a few hundred eV) anisotropic component, and a hot (a few keV) anisotropic distribution. A multicomponent electron model like this has been considered in previous work to explain banded chorus generation [e.g., *Santolík et al.*, 2010], but the temperatures and densities derived from the HOPE measurements are sufficiently different to justify a further study.

Our goal here is to test the hypothesis that banded chorus is due to local linear growth of two branches of the whistler anisotropy instability excited by two distinct, anisotropic electron components of significantly different temperatures using a homogeneous plasma model. While spatially inhomogeneous models of chorus growth are essential to describing some properties of chorus (for example, the characteristic rising tones of certain chorus events are well explained by the nonlinear theory of *Omura et al.* [2009]), our model can provide a physical interpretation for the presence of the distinct frequency bands, the characteristic gap at frequencies near $\Omega_e/2$, and wave properties (i.e., quasi-parallel versus oblique propagation and electromagnetic versus quasi-electrostatic) of each band. This study is not intended to achieve a detailed match between the observations and the simulation results but rather to demonstrate that the banded chorus source hypothesis stated above yields predictions consistent with the observations of this particular event. Elements of linear and nonlinear, inhomogeneous and homogeneous plasma models are probably necessary to give a more complete picture of magnetospheric chorus.

The paper is organized as follows. Section 2 describes our analysis of electron velocity distributions from the Van Allen Probes spacecraft A during a particular banded chorus event, and section 3 describes our use of kinetic dispersion theory [*Gary*, 1993] and PIC simulations [*Liu et al.*, 2011] in a homogeneous, collisionless plasma model to analyze the linear and nonlinear evolution of whistler anisotropy instabilities during this event. Section 4 is a summary and conclusion.

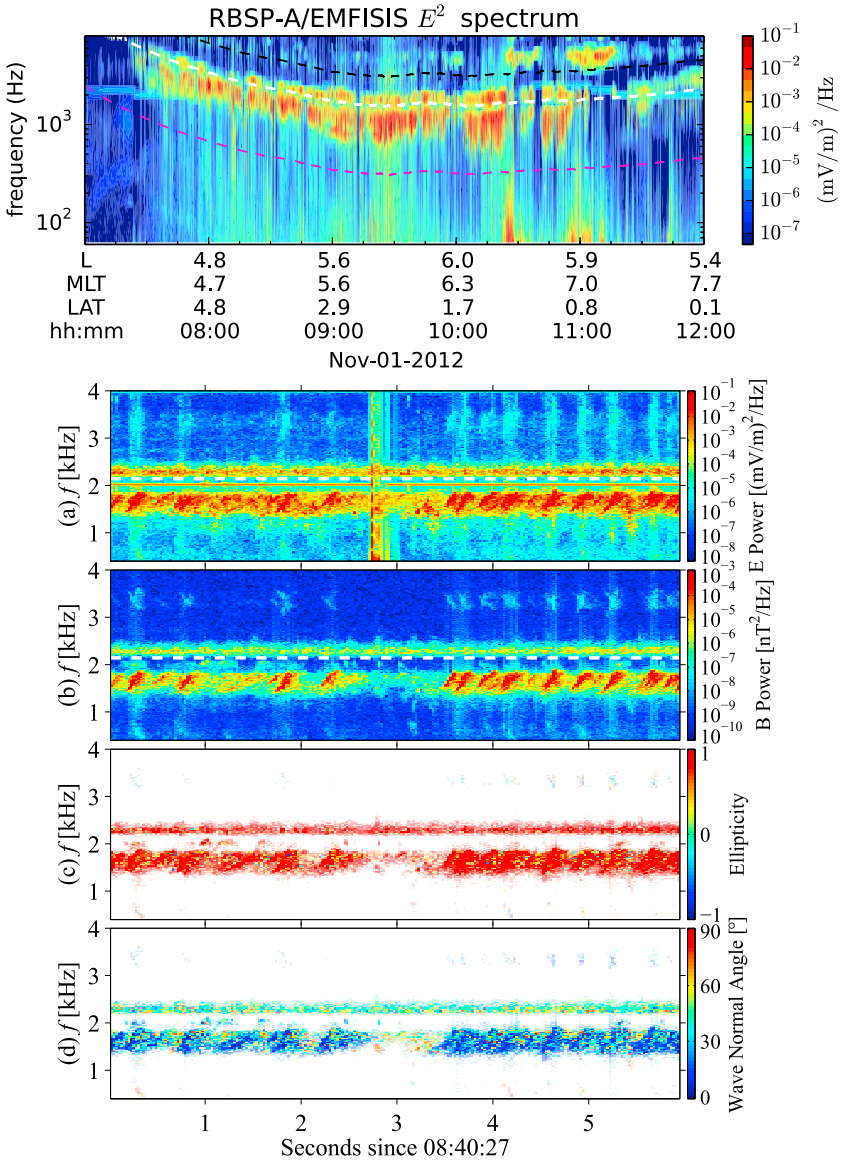

Figure 1. (top) The electric field spectrogram from 7:00 to 12:00 UT on 1 November 2012 as measured by the EMFISIS Waves instrument on Van Allen Probes spacecraft A. Magenta, white, and black curves denote $0.1f_{ce}$, $0.5f_{ce}$, and f_{ce}, respectively. (bottom) The spectrogram of fluctuating (a) electric fields and (b) magnetic fields in the burst mode from 8:40:27 to 8:40:33 UT. A gap appears near half of the local electron cyclotron frequency f_{ce}, denoted by white dashed lines. (c) Ellipticities and (d) propagation angles of the waves. The burst in Figure 1 (bottom, a) is caused by the spike in E_w component due to the shadow of the magnetometer boom; the horizontal line at ~2 kHz is an interference line that may be due with the Electric Field and Waves (EFW) antenna/preamps. Weak second harmonics of the chorus elements at the frequency about 3.5 kHz in Figure 1 (bottom, a and b) were due to the clipping for strong waves before the electric field attenuator was turned on.

2. Van Allen Probes Observations

We here consider Van Allen Probes measurements during the morning of 1 November 2012 associated with a moderate geomagnetic storm with the minimum *Dst* index about −60 nT. Throughout the morning from 8:00 to 11:00 UT, strong banded chorus was observed by Van Allen Probes A on the dawnside near the magnetic equator as shown in Figure 1 (top). Figure 1 (bottom, a and b) shows the spectrograms of the electric and magnetic fluctuations, respectively, measured by the EMFISIS Waves instrument from 8:40:27 to 8:40:33 UT. Two bands of whistler emission are separated by a gap near $\Omega_e/2$ (denoted by the white dashed line), where Ω_e is calculated using local magnetic field strength. The ellipticity and propagation

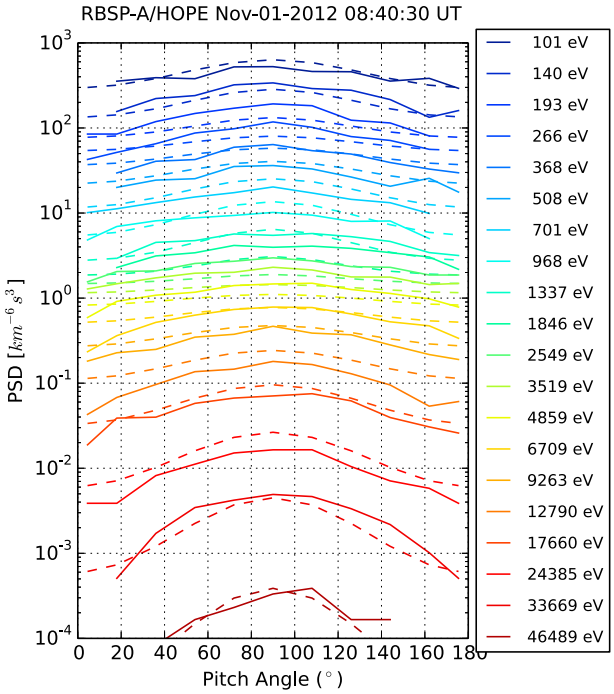

Figure 2. The electron phase space density at 08:40:30 UT on 1 November 2012 measured by the HOPE instrument on Van Allen Probes spacecraft A. The solid lines represent the observed distributions, and the dashed lines show the corresponding fits to a three-component bi-Maxwellian electron model (equation (1)).

angle of waves, as shown in Figure 1 (bottom, c and d), demonstrate that both lower and upper bands have the right-hand polarization characteristic of whistlers but that the lower band propagates at directions quasi-parallel to $\mathbf{B}_o$ with $\theta \leq 20°$ (where θ is the angle between wave number vector **k** and $\mathbf{B}_0$), while the upper band has predominantly oblique propagation, with $40° \leq \theta \leq 60°$. The upper band is quasi-electrostatic, with the propagation angle close to the resonance cone angle $\theta_{\rm res} \approx 57°$ for $\omega = 0.55\Omega_e$, where $\cos\theta_{\rm res} \equiv \omega/\Omega_e$. The combination of parallel lower band and oblique upper band is commonly observed in magnetospheric banded chorus, as shown in several statistical studies [e.g., *Agapitov et al.*, 2012; *Li et al.*, 2013].

The HOPE mass spectrometer measures electron fluxes in five polar angles over energies from 10 eV to 50 keV. We find that throughout the morning of 1 November 2012, the electron velocity distributions measured by HOPE can be approximately represented by the sum of three distinct components: cold (T_c ~ few tens of eV), warm (T_w ~ few hundred eV), and hot (T_h ~ few keV). Electron fluxes measured by HOPE are converted to phase space densities (PSDs), which are then fitted into a three-component bi-Maxwellian distribution function

$$f_M(v_\parallel, v_\perp) = \sum_{j=c,w,h} \sqrt{\frac{m}{2T_{\parallel j}\pi}} \frac{m}{2T_{\perp j}\pi} n_j e^{-\frac{mv_\parallel^2}{2T_{\parallel j}} - \frac{mv_\perp^2}{2T_{\perp j}}}, \quad (1)$$

where c, w, h denote the cold, warm, and hot components, respectively. A nonlinear least squares fitting algorithm has been used to fit PSD data with $\ln(f_M)$. Figure 2 illustrates a typical electron phase space density as a function of pitch angle and energy at 8:40:30 UT where the solid lines correspond to the observations and the dashed lines represent fits to the data with the distribution f_M. The measured distributions are more anisotropic at energies ~200 eV and > 6 keV and more isotropic at intermediate energies around 2 keV. The fitting yields $n_w = 1.02$ cm^{-3} and $n_h = 1.07$ cm^{-3}, $T_{\parallel w} = 256$ eV and $T_{\parallel h} = 4.00$ keV, and $T_{\perp w}/T_{\parallel w} = 1.48$ and $T_{\perp h}/T_{\parallel h} = 1.31$, with the estimated relative standard deviation errors on the parameters less than 4%. Due to relatively high noise levels in low-energy (< 100 eV) measurements, we have chosen not to use the fitting parameters for the cold component. We have also tried fitting the data with a four-component distribution function to reduce the mean square error. However, the linear theory predicts similar properties of the lower and upper band chorus using a four-component model as using a three-component model. Therefore, we restrict ourselves to the three-component model in the rest of the paper.

We have carried out similar fits to the electron velocity distributions for several hours during the morning of 1 November 2012. However, from 9:00 until after 10:30 UT, the spacecraft potential measured by the EFW instrument [*Wygant et al.*, 2013] varies between −50 V and −150 V (also seen in the HOPE proton flux measurements, not shown), which affects the low-energy particle flux measurement and makes it difficult to obtain accurate values of the warm electron component parameters. Therefore, we have focused on the period between 8:00 and 8:50 UT when the spacecraft potential is 20 V or less. Figure 3 shows the nine electron fitting parameters as functions of time between 8:34 and 8:43 UT; during this interval, all nine parameters show relatively small variations. Averaging each parameter over this 9 min interval, we obtain

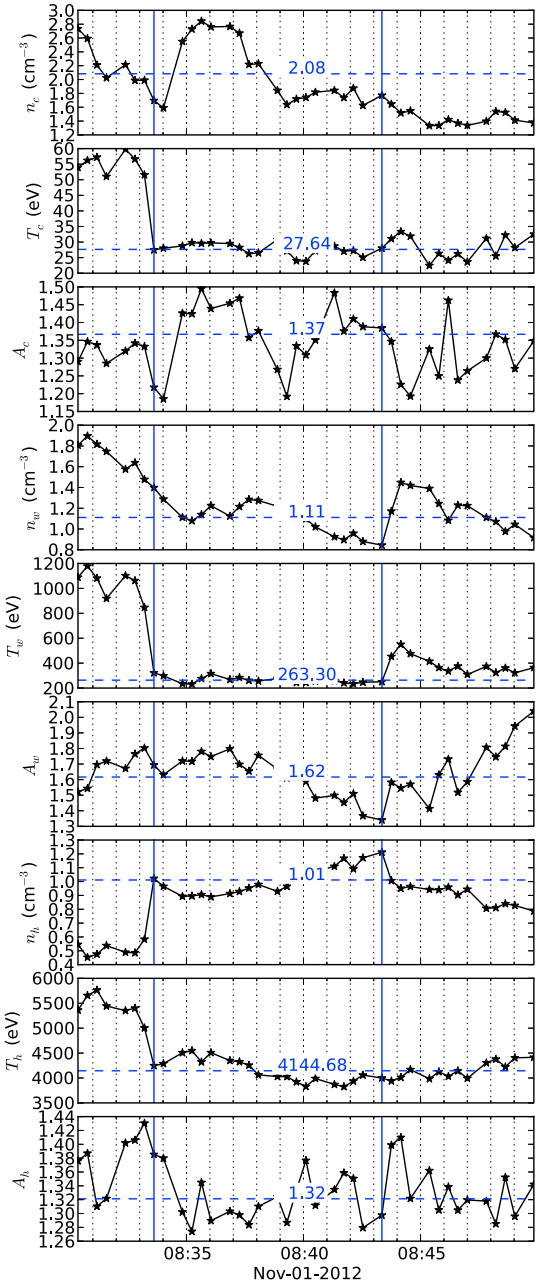

Figure 3. Nine fitting parameters for electron velocity distributions measured from 8:30 to 8:50 UT on 1 November 2012 by the HOPE instrument on Van Allen Probes spacecraft A. The electron component densities and temperatures used as initial conditions in the simulation described in section 3 are the values averaged over the interval from 8:34 to 8:43 (vertical lines).

$n_w = 1.11$ cm^{-3} and $n_h = 1.01$ cm^{-3}, $T_{\|w} = 263$ eV and $T_{\|h} = 4.14$ keV, and $A_w \equiv T_{\perp w}/T_{\|w} = 1.62$ and $A_h \equiv T_{\perp h}/T_{\|h} = 1.32$. During this time, the magnetometer of EMFISIS gives an averaged $B_o \simeq 150$ nT and the averaged total electron density inferred from the upper hybrid emission line, also measured by EMFISIS, is $n_e = 6.1$ cm^{-3}. The density of the cold component is derived by $n_c = n_e - n_w - n_h$, and we obtain $n_c/n_e = 0.65$, $n_w/n_e = 0.18$, $n_h/n_e = 0.17$, $\omega_e/\Omega_e = 5.0$, $\beta_{\|w} = 0.0046$, and $\beta_{\|h} = 0.068$. Here ω_e is the electron plasma frequency, and $\beta_{\|j} = 2\mu_0 n_j T_{\|j}/B_0^2$. Although the instability growth rates are functions of the relative cold plasma density [e.g., *Gary et al.*, 2012], they are independent of a sufficiently small cold electron temperature, which we choose to be 10 eV.

The multicomponent bi-Maxwellian distribution model (equation (1)) used here facilitates the linear analysis and PIC simulations (in section 3). The model works well for most of the time in the 1 November 2012 event in the energy range from a few eV to 50 keV (e.g., Figure 2) and captures the major features of low-energy electron distribution. The observed distributions sometimes may deviate significantly from Maxwellian, especially when the distribution is not monotonically decreasing as a function of $v_\|$ (or E).

3. Particle-in-Cell Simulation

Kinetic linear dispersion theory [*Gary*, 1993] shows that for the observed parameters stated in section 2, the upper band whistler mode is stable and the lower band whistler mode is weakly unstable (maximum growth rate $\gamma_m/\Omega_e < 10^{-4}$; see Figure 4). This is a consequence not only of our averaging the electron parameters over an extended temporal interval but more fundamentally because the rate at which HOPE yields plasma measurements is considerably slower than the presumed electron scattering rate due to enhanced fluctuations from the whistler instabilities. Our PIC simulation allows us to study in detail the instability growth, wave saturation, and electron scattering. The entire chain of processes occurs in less than 1 s even for slow instability growth with $\gamma/\Omega_e = 10^{-3}$. In contrast, the HOPE measurements are limited by the spacecraft spin period which is approximately 10 s; only the average plasma state produced by the full chain of processes is measured. Based on this limitation, we have chosen to start our simulation with initial conditions where the anisotropies of both the warm and hot components are sufficiently large to excite both upper and lower bands of the whistler instability.

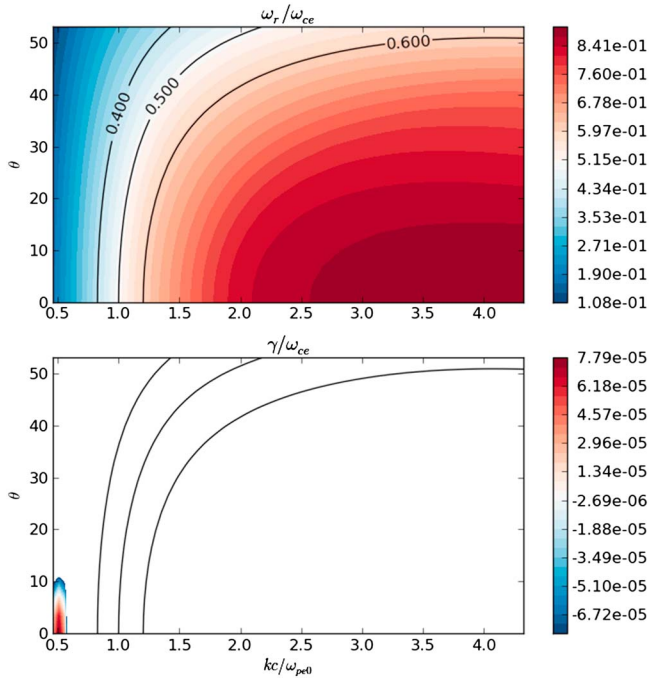

Figure 4. Kinetic linear theory results for (top) whistler anisotropy instability frequencies and (bottom) growth rates as functions of dimensionless wave number k and propagation direction θ using observed parameters as described in the text, including the observed anisotropies $T_{\perp w}/T_{\parallel w} = 1.62$ and $T_{\perp h}/T_{\parallel h} = 1.32$. The three black lines indicate contours of the wave frequencies ω/Ω_e =0.4, 0.5, and 0.6 in the θ-k parameter space.

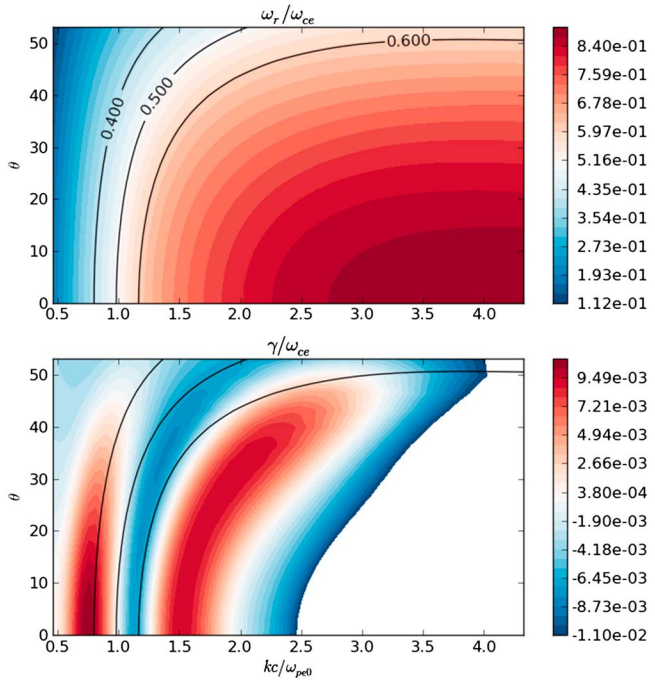

Figure 5. Kinetic linear theory results for (top) whistler anisotropy instability frequencies and (bottom) growth rates using observed parameters except two temperature anisotropies $T_{\perp w}/T_{\parallel w} = 6.0$ and $T_{\perp h}/T_{\perp h} = 2.0$. Similar format as Figure 4.

Our two-dimensional PIC simulation of whistler anisotropy instabilities utilizes the computer code described in *Liu et al.* [2011]. The initial dimensionless parameters are derived from Van Allen Probes measurements as described in the preceding section except that we have chosen enhanced values of the warm and hot component temperature anisotropies: $T_{\perp w}/T_{\parallel w} = 6.0$ and $T_{\perp h}/T_{\parallel h} = 2.0$. These anisotropies are chosen so that the maximum growth rates of both instabilities are about $0.01\Omega_e$ (see Figure 5), which leads to saturation of both instabilities in reasonable simulation time. The initial proton velocity distribution in each case is an isotropic Maxwellian, as is the initial cold electron distribution. The simulation also uses $m_p/m_e = 1836$ and $\omega_e/\Omega_e = 5.1$. With these parameters, linear theory shows that both lower band and upper band whistler modes are unstable; the lower band is electromagnetic with maximum growth rate at parallel propagation, whereas the upper band is quasi-electrostatic with maximum growth at $\theta \simeq 30°$ (see Figure 5).

The simulation domain has size $L_x = L_y = 2.0c/\omega_i$, and the background magnetic field $\mathbf{B}_0$ is in the x direction; 1024×1024 grids are used in the simulation so that $\Delta x = \Delta y = 0.084c/\omega_e$, the time step is $\Delta t = 0.015\Omega_e^{-1}$, and 500 superparticles per species per cell are employed. Periodic boundary conditions for fields and particles are imposed in both directions.

The temporal evolution of several simulation parameters is shown in Figure 6. Figure 6a shows that both the electric and magnetic fluctuations have rapid growth at early times and reach saturation near $t\Omega_e = 1000$. Figure 7 shows power spectrum contours of fluctuating electric and magnetic fields in wave number space taken at $t\Omega_e = 881$ from the simulation. Two groups of waves can be identified: one peaking at $k_\parallel \lambda_e \sim 0.6$, $k_\perp \lambda_e \sim 0$ and one peaking at $k_\parallel \lambda_e \sim 2.3$, $k_\perp \lambda_e \sim 2.3$.

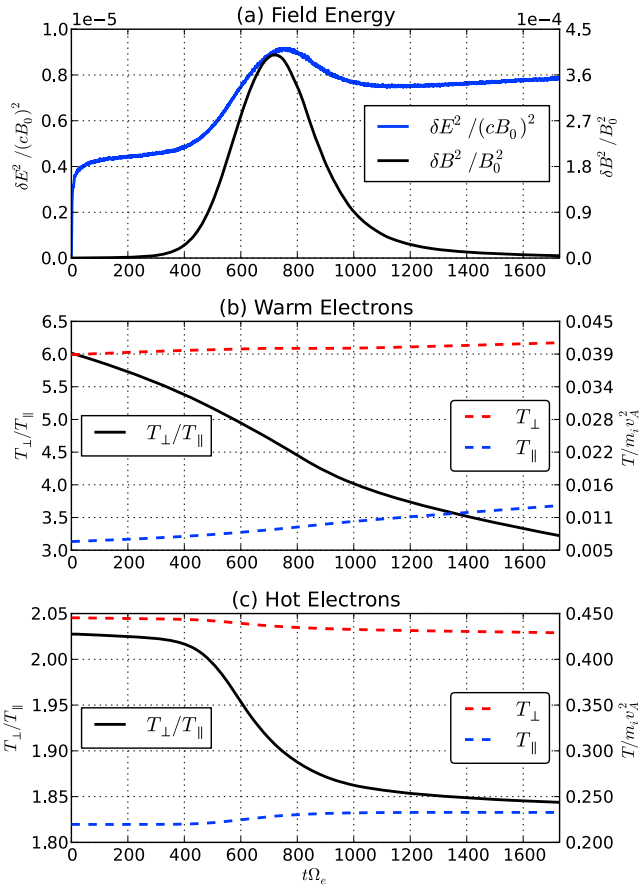

Figure 6. PIC simulation results: The temporal evolution of (a) electric and magnetic field energies, (b) parallel and perpendicular temperatures and the temperature anisotropy of warm electrons, and (c) parallel and perpendicular temperatures and the temperature anisotropy of hot electrons. In the simulation $1000\Omega_e^{-1}$ is approximately 38 ms.

The former group corresponds to the quasi-parallel lower band chorus, and the latter group corresponds to the oblique upper band chorus with $\theta \sim 45°$. These simulation results are consistent with the prediction of linear dispersion theory (Figure 5). If we assume the warm and hot electrons drive waves independently, the difference in propagation of the two bands may be interpreted in terms of *Gary et al.* [2011]; at sufficiently large component $\beta_\parallel$, the unstable modes are electromagnetic with maximum growth at parallel propagation and $\omega_r \leq 0.5\Omega_e$, whereas at sufficiently small component $\beta_\parallel$, growing waves are quasi-electrostatic with maximum growth at $40° < \theta < 50°$ and $\omega_r > 0.5\Omega_e$. However, in contrast to *Liu et al.* [2011], here we used observed temperatures and densities of electron components, which affect the linear properties of both bands and wave-particle interactions. For example, when the temperatures of two components are close as in this paper, there is weak cyclotron resonance of warm electrons with the lower band whistler waves so that the growth rate of the upper band depends also on parameters of hot electrons (which drive the lower band).

Figures 6b and 6c illustrate the responses of the warm and the hot electron components to the growth and subsequent decay of the fluctuating fields. These fields scatter both components so as to reduce their temperature anisotropies, with A_h from 2.0 down to 1.85 and A_w from 6.0 down to 3.3 (A_w is still decreasing at the end of the simulation). These anisotropies are greater than, but approaching, the observed values. Our simulation reinforces basic results of *Liu et al.* [2011]: that the warm and hot components drive the upper and lower chorus bands, respectively, and that at least through time of saturation linear instability growth determines the dynamics with no evidence for nonlinear coupling between the spectra of the two bands [cf. *Schriver et al.*, 2010]. Our simulation also reinforces fundamental conclusions of *Gary et al.* [2011] that electromagnetic whistler fluctuations reduce the electron component anisotropy through pitch angle scattering, whereas quasi-electrostatic whistlers can scatter electrons into the high-speed tail of the parallel velocity distribution through Landau resonance.

We have also carried out a series of simulations by varying the initial anisotropies: $A_w = 5, 6, 8$, and 10 and $A_h = 3, 4$, and 5. We found that with larger initial anisotropies, stronger waves can be excited, which scatter the electrons more rapidly, resulting in a reduced late-time anisotropy as shown in Figure 8. This effect of enhanced scattering and reduced final anisotropy with increasing initial anisotropy is consistent with previous work [e.g., *Gary and Wang*, 1996]. In this study we choose not to adjust the initial parameters so that we match the end state of the simulation to the observed values for a few reasons. First, the mechanism for producing such high anisotropies is still unclear. Second, our PIC simulations are able to run for only a short period of time (~0.1 s); in the much longer times available in the actual plasma, the waves may persist, further scattering electrons and reducing the anisotropies, although at a much lower rate. Third, with

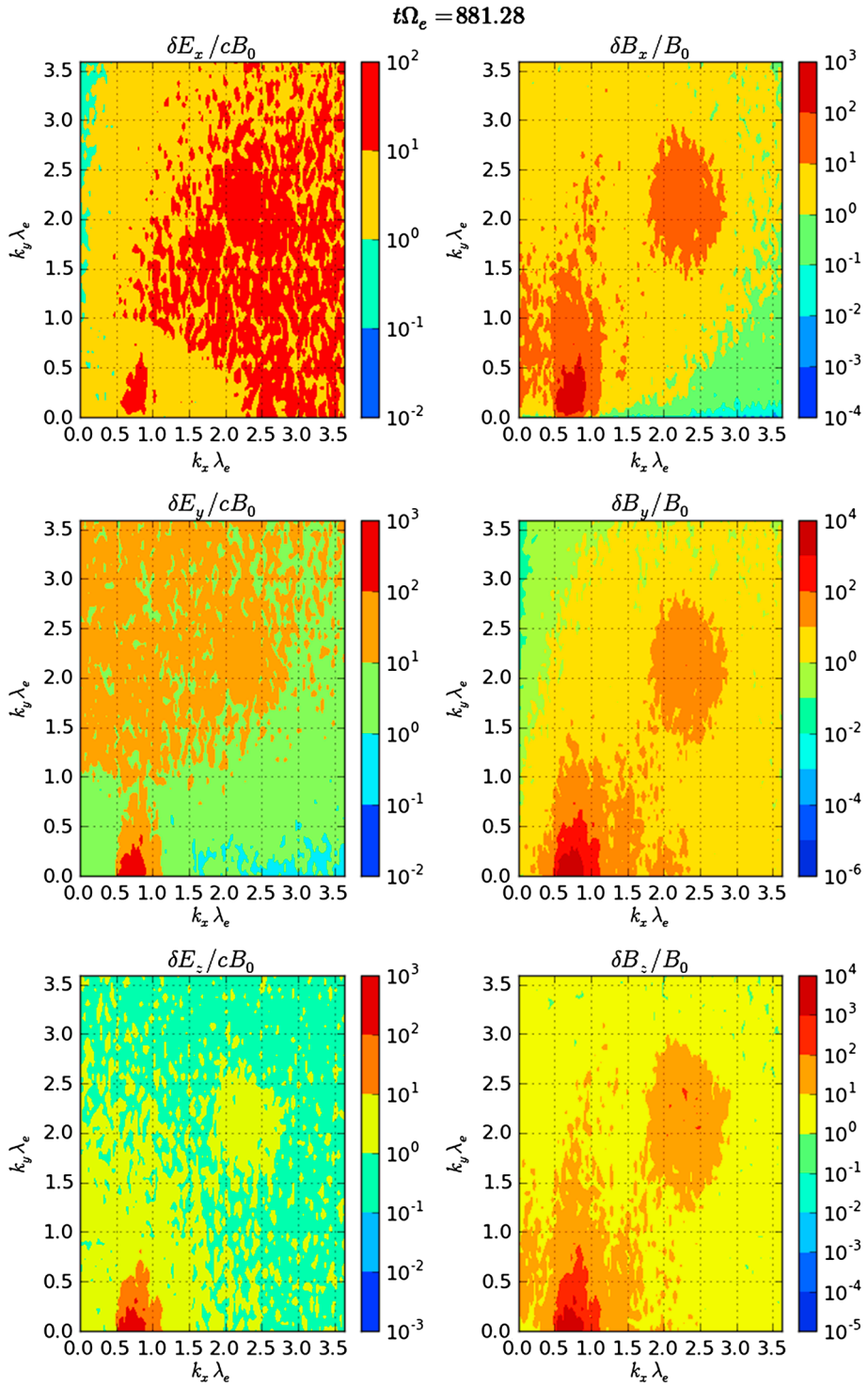

Figure 7. PIC simulation results: **k** spectra of late-time ($t\Omega_e = 881$) fluctuating fields. (left) Electric and (right) magnetic field energy densities for the three components as functions of $k_x(k_\parallel)$ and $k_y(k_\perp)$.

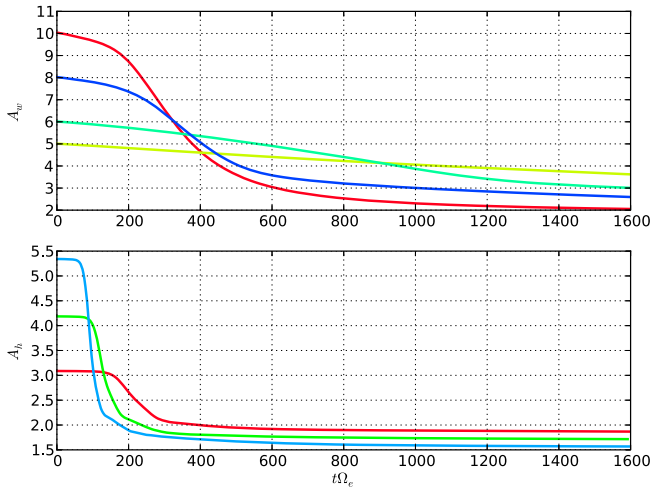

Figure 8. A series of PIC simulations with different initial temperature anisotropies $A_w = 5, 6, 8$, and 10 and $A_h = 3, 4$, and 5 (due to relativistic effect, calculated initial A_h's shown in the figure are slightly larger than prescribed values). For each run shown here, all parameters are the same as for the simulation described in section 3 except for the indicated anisotropies of the warm or hot electrons.

large initial anisotropies (e.g., $A_w = 10, A_h = 3$), strong and broadband waves are excited so that the gap between the lower band and the upper band becomes vague. The hypothesis is more clearly confirmed when instabilities for both bands are close to their thresholds. It is also possible that injections of warm and hot electrons are highly localized in space and/or time so that the observed anisotropies (averaged over 10 s) are even lower than the time-averaged values in the PIC simulation. Such localization may also explain the observed temporal separation of chorus signals.

Figure 9 shows frequency spectra of δE_y and δB_y signals at the center of the simulation box over $600 \le t\Omega_e \le 1400$. There is a clear separation at $\omega_r \simeq \Omega_e/2$ between the lower band with frequency $0.25 \le \omega_r/\Omega_e \le 0.45$ and the upper band with frequency $0.60 \le \omega_r/\Omega_e \le 0.75$. The ratio of $|\delta E_y/\delta B_y|$ for the upper band is much greater than that for the lower band, indicating that the upper band is more electrostatic and the lower band is electromagnetic. This is consistent with the k spectrum analysis (Figure 7) showing that the upper band is at oblique propagation and the lower band is quasi-parallel. The fluctuating field spectra in our simulations for both bands are broad compared to typical observations in the magnetosphere [e.g., *Bunch et al.*, 2013]; and the upper band peaks at $0.7\Omega_e$, which is higher than the observed peak at $0.5–0.6\Omega_e$ [e.g., *Meredith et al.*, 2009]. This may be due to the initial Maxwellian distributions (equation (1)) we used in the simulation. Narrowband chorus could be generated by enhanced electron flux anisotropy in a narrow energy range as is evident from the resonance condition $\omega - k_\parallel v_\parallel = \Omega_e$. The peak frequency of the upper band can be lower if the parallel temperature of the warm electrons increases, as shown by *Gary et al.* [2011].

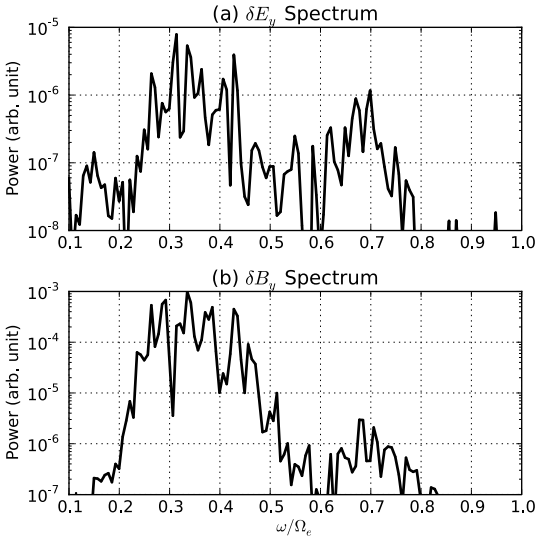

Figure 9. PIC simulation results: Frequency spectra of (a) electric field δE_y and (b) magnetic field δB_y fluctuations over $600 \le t\Omega_e \le 1400$.

Due to the limitation of computing resources, we used a relatively small periodic simulation box with homogeneous background magnetic field in this study. Therefore, propagation effects and nonlinear effects due to magnetic field inhomogeneity are not included. These effects may be important in explaining other features of observed chorus, such as the rising tones [*Omura et al.*, 2009]. As simulation techniques advance, future PIC simulations with larger simulation domains and more realistic magnetic field configuration will be able to address these issues.

4. Conclusions

We have used PIC simulations to examine whistler anisotropy instability growth in a magnetized, homogeneous, collisionless plasma using plasma and field

parameters derived from Van Allen Probes measurements of a banded chorus event on 1 November 2012. The electrons are represented as three components: a cold isotropic component, a warm anisotropic component, and a hot anisotropic component. As in previous PIC simulations [*Liu et al.*, 2011], sufficiently large anisotropies on the warm and hot populations drive upper and lower band whistler instabilities, respectively. The upper band instability is driven at $0.60 \leq \omega_r \leq 0.75\Omega_e$, whereas the lower band instability typically arises at $0.25 \leq \omega_r/\Omega_e \leq 0.45$ so that as long as the two electron component anisotropies are sensibly above instability thresholds, the fluctuating field spectra exhibit a gap near $\Omega_e/2$. The results confirm the hypothesis that the banded chorus characteristic gap near $\Omega_e/2$ may be explained as the consequences of local, linear whistler instability growth driven by two distinct, anisotropic electron components of significantly different temperatures. We focused on the generation mechanism of banded chorus without propagation effects or inhomogeneity of the background magnetic field.

Another advantage of the hypothesis of banded chorus excitation is that it can be adapted to explain other types of chorus—lower band only, upper band only, or even a broadband without the gap at $\Omega_e/2$— by limiting the number of unstable electron components and changing their temperatures. A recent study by *Su et al.* [2014], showing that a lower band chorus observed also by Van Allen Probes was associated with anisotropic electron fluxes at energies above a few keV (what we call a hot component), is consistent with the hypothesis. A statistical study of more chorus events of different types and their correlation with electron pitch angle distributions would further test the validity of the hypothesis.

A more complete picture of banded chorus generation will also require understanding the physical mechanisms/processes that can generate highly anisotropic electron populations used in this paper. A recent study by *Birn et al.* [2014] using MHD simulations with test particle tracing showed that high-temperature anisotropies of electrons may be produced in the process of magnetotail reconnection, burst flows, and dipolarization. This result, although it cannot be applied to our study directly (because *Birn et al.* [2014] only trace electrons to ~10 R_E on the nightside), has made potential progress in this direction.

Acknowledgments

The Los Alamos portion of this research was performed under the auspices of the U.S. Department of Energy. This research was supported in part by the Defense Threat Reduction Agency, by the National Aeronautics and Space Administration, and by the National Science Foundation. The work at the University of Iowa was supported by JHU/APL through contract 921647 under NASA Prime contract NAS5-01072. S.P.G.'s contributions to this research were supported by NSF award AGS-1303300. The work at Auburn University was supported by NASA grant NNX14AD62G.

Michael Balikhin thanks Binbin Ni and Didier Mourenas for their assistance in evaluating this paper.

References

Agapitov, O., V. Krasnoselskikh, Y. V. Khotyaintsev, and G. Rolland (2012), Correction to "A statistical study of the propagation characteristics of whistler waves observed by Cluster", *Geophys. Res. Lett.*, *39*, L24102, doi:10.1029/2012GL054320.

Bell, T. F., U. S. Inan, N. Haque, and J. S. Pickett (2009), Source regions of banded chorus, *Geophys. Res. Lett.*, *36*, L11101, doi:10.1029/2009GL037629.

Birn, J., A. Runov, and M. Hesse (2014), Energetic electrons in dipolarization events: Spatial properties and anisotropy, *J. Geophys. Res. Space Physics*, *119*, 3604–3616, doi:10.1002/2013JA019738.

Bunch, N. L., M. Spasojevic, Y. Y. Shprits, X. Gu, and F. Foust (2013), The spectral extent of chorus in the off-equatorial magnetosphere, *J. Geophys. Res. Space Physics*, *118*, 1700–1705, doi:10.1029/2012JA018182.

Funsten, H. O., et al. (2013), Helium, Oxygen, Proton, and Electron (HOPE) mass spectrometer for the radiation belt storm probes mission, *Space Sci. Rev.*, *179*, 423–484, doi:10.1007/s11214-013-9968-7.

Gary, S. P. (1993), *Theory of Space Plasma Microinstabilities*, Cambridge Atmospheric and Space Science Series, Cambridge Univ. Press, Cambridge, U. K.

Gary, S. P., and J. Wang (1996), Whistler instability: Electron anisotropy upper bound, *J. Geophys. Res.*, *101*, 10,749–10,754.

Gary, S. P., K. Liu, and D. Winske (2011), Whistler anisotropy instability at low electron β: Particle-in-cell simulations, *Phys. Plasmas*, *18*(8), 082902, doi:10.1063/1.3610378.

Gary, S. P., K. Liu, R. E. Denton, and S. Wu (2012), Whistler anisotropy instability with a cold electron component: Linear theory, *J. Geophys. Res.*, *117*, A07203, doi:10.1029/2012JA017631.

Habagishi, T., S. Yagitani, and Y. Omura (2014), Nonlinear damping of chorus emissions at local half cyclotron frequencies observed by Geotail at L > 9, *J. Geophys. Res. Space Physics*, *119*, 4475–4483, doi:10.1002/2013JA019696.

Kletzing, C. A., et al. (2013), The Electric and Magnetic Field Instrument Suite and Integrated Science (EMFISIS) on RBSP, *Space Sci. Rev.*, *179*(1–4), 127–181, doi:10.1007/s11214-013-9993-6.

Kurita, S., Y. Katoh, Y. Omura, V. Angelopoulos, C. M. Cully, O. Le Contel, and H. Misawa (2012), THEMIS observation of chorus elements without a gap at half the gyrofrequency, *J. Geophys. Res.*, *117*, A11223, doi:10.1029/2012JA018076.

Li, W., et al. (2010), THEMIS analysis of observed equatorial electron distributions responsible for the chorus excitation, *J. Geophys. Res.*, *115*, A00F11, doi:10.1029/2009JA014845.

Li, W., J. Bortnik, R. M. Thorne, C. M. Cully, L. Chen, V. Angelopoulos, Y. Nishimura, J. B. Tao, J. W. Bonnell, and O. LeContel (2013), Characteristics of the Poynting flux and wave normal vectors of whistler-mode waves observed on THEMIS, *J. Geophys. Res. Space Physics*, *118*, 1461–1471, doi:10.1002/jgra.50176.

Liu, K., P. S. Gary, and D. Winske (2011), Excitation of banded whistler waves in the magnetosphere, *Geophys. Res. Lett.*, *38*, L14108, doi:10.1029/2011GL048375.

MacDonald, E. A., M. H. Denton, M. F. Thomsen, and S. P. Gary (2008), Superposed epoch analysis of a whistler instability criterion at geosynchronous orbit during geomagnetic storms, *J. Atmos. Sol. Terr. Phys.*, *70*(14), 1789–1796, doi:10.1016/j.jastp.2008.03.021.

Meredith, N. P., R. B. Horne, and R. R. Anderson (2001), Substorm dependence of chorus amplitudes: Implications for the acceleration of electrons to relativistic energies, *J. Geophys. Res.*, *106*, 13,165–13,178.

Meredith, N. P., R. B. Horne, R. M. Thorne, and R. R. Anderson (2009), Survey of upper band chorus and ECH waves: Implications for the diffuse aurora, *J. Geophys. Res.*, *114*, A07218, doi:10.1029/2009JA014230.

Meredith, N. P., R. B. Horne, A. Sicard-Piet, D. Boscher, K. H. Yearby, W. Li, and R. M. Thorne (2012), Global model of lower band and upper band chorus from multiple satellite observations, *J. Geophys. Res.*, *117*, A10225, doi:10.1029/2012JA017978.

Omura, Y., M. Hikishima, Y. Katoh, D. Summers, and S. Yagitani (2009), Nonlinear mechanisms of lower-band and upper-band VLF chorus emissions in the magnetosphere, *J. Geophys. Res.*, *114*, A07217, doi:10.1029/2009JA014206.

Reeves, G. D., et al. (2013), Electron acceleration in the heart of the Van Allen radiation belts, *Science*, *341*(6149), 991–994, doi:10.1126/science.1237743.

Santolík, O., D. A. Gurnett, J. S. Pickett, M. Parrot, and N. Cornilleau-Wehrlin (2003), Spatio-temporal structure of storm-time chorus, *J. Geophys. Res.*, *108*(A7), 1278, doi:10.1029/2002JA009791.

Santolík, O., et al. (2010), Wave-particle interactions in the equatorial source region of whistler-mode emissions, *J. Geophys. Res.*, *115*, A00F16, doi:10.1029/2009JA015218.

Santolík, O., C. A. Kletzing, W. S. Kurth, G. B. Hospodarsky, and S. R. Bounds (2014), Fine structure of large-amplitude chorus wave packets, *Geophys. Res. Lett.*, *41*, 293–299, doi:10.1002/2013GL058889.

Sazhin, S. S., and M. Hayakawa (1992), Magnetospheric chorus emissions: A review, *Planet. Space Sci.*, *40*(5), 681–697.

Schriver, D., et al. (2010), Generation of whistler mode emissions in the inner magnetosphere: An event study, *J. Geophys. Res.*, *115*, A00F17, doi:10.1029/2009JA014932.

Spence, H. E., et al. (2013), Science goals and overview of the Radiation Belt Storm Probes (RBSP) Energetic Particle, Composition, and Thermal Plasma (ECT) suite on NASA's Van Allen Probes mission, *Space Sci. Rev.*, *179*, 311–336, doi:10.1007/s11214-013-0007-5.

Su, Z., et al. (2014), Intense duskside lower band chorus waves observed by Van Allen Probes: Generation and potential acceleration effect on radiation belt electrons, *J. Geophys. Res. Space Physics*, *119*, 4266–4273, doi:10.1002/2014JA019919.

Thorne, R. M. (2010), Radiation belt dynamics: The importance of wave-particle interactions, *Geophys. Res. Lett.*, *37*, L22107, doi:10.1029/2010GL044990.

Thorne, R. M., B. Ni, X. Tao, R. B. Horne, and N. P. Meredith (2010), Scattering by chorus waves as the dominant cause of diffuse auroral precipitation, *Nature*, *467*(7318), 943–946, doi:10.1038/nature09467.

Thorne, R. M., et al. (2013), Rapid local acceleration of relativistic radiation-belt electrons by magnetospheric chorus, *Nature*, *504*(7480), 411–414, doi:10.1038/nature12889.

Wygant, J. R., et al. (2013), The electric field and waves instruments on the radiation belt storm probes mission, *Space Sci. Rev.*, *179*(1–4), 183–220, doi:10.1007/s11214-013-0013-7.